CHEMISTRY
AN ASIAN JOURNAL

DOI: 10.1002/asia.200700068

A DFT Study on the Mechanism of $Rh_2^{II,II}$-Catalyzed Intramolecular Amidation of Carbamates

Xufeng Lin,[a] Cunyuan Zhao,[b] Chi-Ming Che,*[a] Zhuofeng Ke,[b] and David Lee Phillips[a]

Abstract: The potential-energy surfaces of the reactions of dirhodium tetracarboxylate ($Rh_2^{II,II}$) catalyzed nitrene (NR) insertion into C–H bonds were examined by a DFT computational study. A pure Becke exchange functional (B88) rather than a hybrid exchange functional (B3, BHandH) was found to be appropriate for the calculation of the energy difference between the singlet and triplet $Rh_2^{II,II}$–NH nitrene species. $Rh_2^{II,II}$–NR^1 (R^1 = (*S*)-2-methyl-1-butylformyl) is thermodynamically more favorable with a free energy lower than that of $Rh_2^{II,II}$–N-(PhI)R^1. The singlet and triplet states of $Rh_2^{II,II}$–NR^1 have similar stability. Singlet $Rh_2^{II,II}$–NR^1 undergoes a concerted NR insertion into the C–H bond with simultaneous formation of the N–H and N–C bonds during C–H bond cleavage; triplet $Rh_2^{II,II}$–NR^1 undergoes H atom abstraction to produce a diradical, followed by subsequent bond formation by diradical recombination. The singlet pathway is favored over the triplet in the context of the free energy of activation and leads to the retention of the chirality of the C atom in the NR insertion product. The reactivities of the C–H bonds toward the nitrene-insertion reaction follow the order tertiary > secondary > primary. Relative reaction rates were calculated for the six reaction pathways examined in this work.

Keywords: amidation · density functional calculations · nitrene insertion · reaction mechanisms · rhodium

Introduction

Catalytic C–H bond amination involving nitrenes (NR) is developing into an important alternative to classical methods of C–N bond formation, and this is attractive for building functionalized amines.[1–3] Since the pioneering work of Breslow and Gellman in the 1980s,[4,5] considerable advances in this area have been made, and various transition-metal catalysts, including those that contain Fe,[4–6] Cu,[7–9] Rh,[5,10–17] Mn,[6,18–21] and Ru[22–25] atoms with diverse ligand scaffolds, have been reported for catalytic intramolecular C–H bond amination. Metal-catalyzed C–N bond-formation reactions can be regio- and stereoselective. Despite extensive studies on their synthetic applications, mechanistic investigations of intramolecular nitrene C–H insertions are rare. Imino phenyliodinanes (PhI=NR) are often used as a "nitrene source" for the generation of the reactive "metal–nitrene" intermediate, whereas the actual intermediate(s) directly responsible for NR insertion into C–H bonds remains elusive in the literature. Both metal–phenyliodinane (L_xM–N(IPh)R)[4–6,20,26] and metal–nitrene (L_xM–NR)[9,16] intermediates have been suggested to be responsible for NR-group delivery,[27] and concerted insertion via a singlet nitrenoid or radical recombination via a triplet nitrenoid may be feasible pathways in the C–N bond-formation reactions.[16] In stoichiometric intermolecular C–H bond amidation by Ru–imido[18,22,28] and C–H bond amidation catalyzed by Mn–porphyrin complexes,[20] a carboradical reactive intermediate was proposed in each case. In contrast, Espino and Du Bois proposed that a concerted insertion process is responsible for dirhodium(II,II)-catalyzed intramolecular amidations.[13] Generally, the nitrene (NR) group preferentially inserts into tertiary and benzylic C–H bonds.[1,3,14]

[a] X. Lin, Prof. C.-M. Che, Prof. Dr. D. L. Phillips
Department of Chemistry and
Open Laboratory of Chemical Biology of the
Institute of Molecular Technology for Drug Discovery and Synthesis
The University of Hong Kong
Pokfulam Road, Hong Kong (China)
Fax: (+852) 2857-1586
E-mail: cmche@hku.hk

[b] Prof. C. Zhao, Z. Ke
School of Chemistry and Chemical Engineering
Sun Yat-Sen University
Guangzhou 510275 (China)

Supporting information for this article is available on the WWW under http://www.chemasianj.org or from the author.

 © 2007 Wiley-VCH Verlag GmbH & Co. KGaA, Weinheim

Among the transition-metal complexes reported to catalyze nitrene insertion into C–H bonds, the dirhodium carboxylates (denoted $Rh_2^{II,II}$ hereafter) have been demonstrated by Du Bois and co-workers to be versatile catalysts in most C–N bond formations.[10–17] Nakamura et al.[29] reported a computational study of $Rh_2^{II,II}$-catalyzed carbene insertion into the C–H bonds of hydrocarbons, but there has been no analogous study of C–N bond formation involving $Rh_2^{II,II}$ catalysts. In recent years, Du Bois and co-workers reported the synthesis of a series of oxazolidinones[13] and oxathiazinanes[12,14,15] from carbamates and sulfamates, respectively, by intramolecular nitrene insertion into C–H bonds with $Rh_2^{II,II}$ as a catalyst. Herein we report a density functional theory (DFT) computational study of the $Rh_2^{II,II}$-catalyzed intramolecular C–H bond-amidation reactions that were previously reported in reference [13]. Our results show that "$Rh_2^{II,II}$–nitrene" is the active species directly responsible for nitrene insertion into the C–H bond. The singlet and triplet "$Rh_2^{II,II}$–nitrene" studied in this work have similar thermodynamic stability, but the C–N bond formation comes from a concerted singlet-nitrene-insertion pathway.

It has been generally assumed that $Rh_2^{II,II}$-mediated intramolecular aminations involve the following steps: in situ generation of imino phenyliodinanes from the substrate(s), formation of the active intermediate(s) from $Rh_2^{II,II}$, which is responsible for delivery of the NR group, and C–H activation/C–N bond formation (Scheme 1). In this study, $Rh_2(O_2CH)_4$ (**1**; Figure 1) was used to model the $Rh_2(O_2CCH_3)_4$ catalyst. (*S*)-2-methyl-1-butyl carbamate was chosen as a model substrate to examine the mechanism of the intramolecular amidations reported in reference [13].

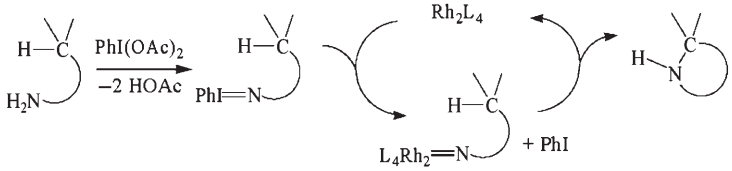

Scheme 1. Catalytic cycle for $Rh_2^{II,II}$-mediated intramolecular amidation reactions.

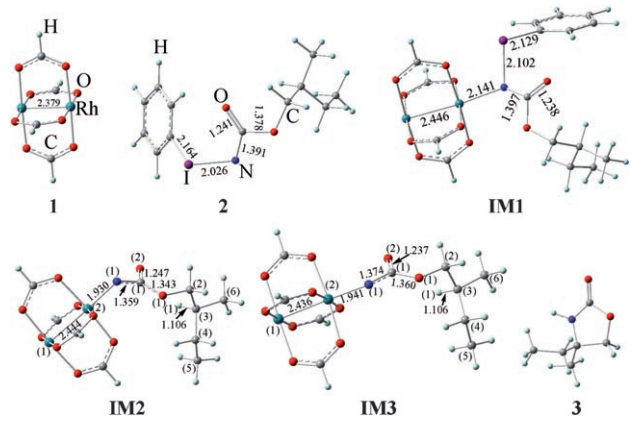

Figure 1. Optimized structures at the BPW91/BS1 level for $Rh_2^{II,II}$ (**1**), imino phenyliodinane (**2**), $Rh_2^{II,II}$–phenyliodinane intermediate **IM1**, $Rh_2^{II,II}$–NR^1 intermediates **IM2** (singlet) and **IM3** (triplet), and the final oxazolidinone product (**3**). Key bond lengths and distances (Å) are indicated. Atom symbols are indicated on selected atoms for clarity.

Results and Discussion

E_{st} of $Rh_2^{II,II}$–NH Complex with Different Computational Methods

The energy difference between the singlet and triplet states (E_{st}) is usually an issue of discussion in nitrene chemistry.[30] Although hybrid functionals, especially B3LYP,[31] are popular in DFT calculations, it was reported that B3LYP often overestimates E_{st} by about 8–10 kcal mol^{-1} for some nitrenes, such as acylnitrene,[32,33] compared to that obtained at the more accurate CCSD(T) level of computation. The pure Becke exchange functional[34] may lead to a more accurate E_{st} value[35] that is comparable to that observed in experimental results.[36] In this work, we carefully chose an appropriate set of exchange and correlation functionals when using DFT methods. Table 1 shows the E_{st} values for the $Rh_2^{II,II}$–NH species (Figure 2) obtained with different computational methods and basis-set levels. It was found that different correlation functionals did not significantly affect the E_{st} value; instead, different exchange functionals did have an effect. The E_{st} value predicted by the B3 (B3LYP and B3PW91) methods were around 13 kcal mol^{-1} in each case, whereas the BHandH[37] method predicted a value of around 26 kcal mol^{-1}. The pure Becke exchange methods (BPW91, BLYP) predicted values lower than 3 kcal mol^{-1}, which is similar to the result obtained by CCSD(T) single-point calculations. The exchange functional that contains a larger contribution from the Hartree–Fock exchange would lead to a larger deviation than in the CCSD(T) results. As revealed in Table 1, the E_{st} value computed with a higher basis-set level (BS3; see the designation of BS1–BS3 in the Computational Details) is rather close to that computed with a lower level (BS1). Furthermore, the calculated geometric parameters of the $Rh_2(O_2CH)_4$ model are similar to those obtained by X-ray crys-

Table 1. The singlet and triplet energy split ($E_{st}=E_{singlet}-E_{triplet}$) of the $Rh_2^{II,II}$–NH complex with different computational methods and basis-set levels.

Method/basis set	CCSD(T)/BS2//BPW91/BS1	CCSD(T)/BS2//B3LYP/BS1	BPW91/BS3
E_{st} [kcal mol^{-1}]	1.4	2.4	2.6

Method/basis set	BPW91/BS1	BLYP/BS1	B3PW91/BS1	B3LYP/BS1	BHandH/BS1	HF/BS1
E_{st} [kcal mol^{-1}]	2.9	2.6	13.2	12.9	25.7	86.9

 © 2007 Wiley-VCH Verlag GmbH & Co. KGaA, Weinheim

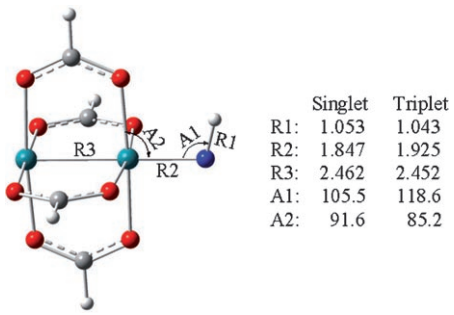

Figure 2. Optimized structures at the BPW91/BS1 level for the $Rh_2^{II,II}$–NH complex. Key bond lengths (Å) and angles (°) are indicated.

tallography.[38] Therefore, the BPW91/BS1 method was used in the following computational study.

Formation and Decomposition of $Rh_2^{II,II}$–Phenyliodinane Complex

Taking into account the controversy of whether a metal–phenyliodinane (L_xM–N(IPh)R) or a metal–nitrene (L_xM–NR) is directly responsible for the nitrene delivery, we examined the thermodynamic stability of these two species compared to that of the starting materials (SM), that is, $Rh_2(O_2CH)_4$ (**1**) and carbonylimino phenyliodinane (**2**), of which the latter is generated in situ from (*S*)-2-methylbutyl carbamate.[3,13] As shown in Figure 3, an $Rh_2^{II,II}$–phenyliodinane complex, denoted **IM1**, can be formed from **1** and **2** with ΔE and ΔG values of −21.8 and −8.3 kcal mol^{-1}, respectively. As revealed by the structure of **IM1**, the formation of the Rh–N bond is associated with elongation of the Rh–Rh bond from 2.379 to 2.446 Å and a weaker interaction between the N and I atoms (the N–I bond length increased from 2.026 to 2.102 Å). From a localized-orbital analysis,[39] one can see that back-donation from the Rh $4d_{xz}$ orbital to the N–I σ* orbital (see the local orbital LO1 of **IM1**, Figure 4e) may play an important role in driving the PhI detachment.[29,40,41] As depicted in Figure 3, the subsequent decomposition of **IM1** to **IM2/IM3** and PhI is greatly favored by a large negative ΔG value (−11.7 and −13.2 kcal mol^{-1} for **IM2** and **IM3**, respectively). Here **IM2** and **IM3** refer to singlet and triplet $Rh_2^{II,II}$–nitrene, respectively, and they have similar thermodynamic stability (see below). As the energy of **IM1** is similar to that of **IM2**+PhI, the decomposition of **IM1** to **IM2**+PhI is a consequence of the increase in entropy. These results indicate that the "metal–nitrene" may possibly serve as the active species for delivery of the NR group.

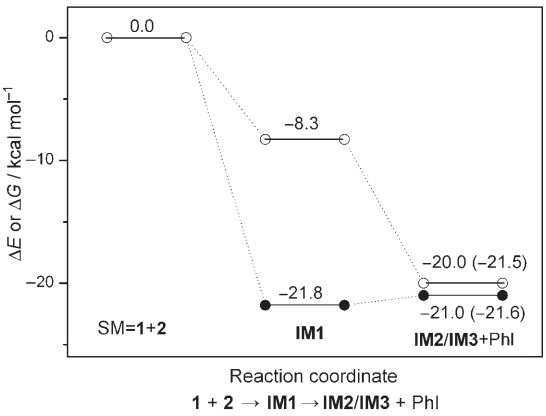

Figure 3. Relative energy (ΔE) and free energy (ΔG) profiles for the Rh-mediated decomposition of imino phenyliodinanes. Values in parentheses correspond to **IM3**. ΔG data were obtained at 313.15 K throughout this paper.[13] ● = *E* profile, ○ = *G* profile.

N-Atom Insertion into C–H Bond via $Rh_2^{II,II}$–NR Complex: Singlet versus Triplet Pathways

Considering that the reaction mechanisms of NR-group insertion for the singlet and triplet metal–nitrene species are different, we estimated the relative thermodynamic stability of singlet and triplet $Rh_2^{II,II}$–nitrene, that is, **IM2** and **IM3**, respectively. The energy/free-energy differences between **IM2** and **IM3** obtained by different computational methods are listed in Table 2. The E_{st} and G_{st} values are within 1.5 kcal mol^{-1}, which indicate that the singlet and triplet $Rh_2^{II,II}$–nitrenes could be present at similar concentrations in the reaction system. This hypothesis is strengthened by a Kohn–Sham orbital analysis.[42]

Table 2. E_{st} and G_{st} values for the singlet intermediate **IM2** and the triplet intermediate **IM3**.

Method/basis set	BPW91/BS1	BPW91/BS1/DPCM	BPW91/BS3/DPCM//BPW91/BS1
$E_{st}=E_{IM2}-E_{IM3}$	0.6	0.3	0.5
$G_{st}=G_{IM2}-G_{IM3}$	1.5	1.4	1.5

It is well-documented that a common free nitrene (NR) or carbene (CR_2) is more stable in the triplet state than in the singlet state without π donation of the R group. This is because the two singly occupied π oribitals of the N/C atoms are degenerate,[30] and according to the Hund principle, an additional paired energy is needed to form a singlet nitrene/carbene species; thus, $E_{st}=E_{singlet}-E_{triplet}=E_{paired}$. Inspection of the frontier orbitals, that is, the HOMO and LUMO of singlet **IM2** (Figure 4a and b) and the two singly occupied molecular orbitals (SOMOs; $E_{SOMO1}<E_{SOMO2}$) of triplet **IM3** (Figure 4c and d) showed that all of these orbitals are antibonding and involve a combination between the N π and Rh–Rh π* orbitals. On the basis of the MO coefficients, LUMO/SOMO2 of **IM2/IM3** has a larger contribution from the N 2p orbital than HOMO/SOMO1. This indicates that the two degenerate π orbitals of the N atom in the free nitrene overlap differently with the Rh–Rh π* orbitals, thus leading to the energy splitting (E_Δ) of these two frontier orbitals. E_Δ favors the singlet over the triplet state from the equation $E_{st}=E_{paired}-E_\Delta$. As a consequence, **IM2** and **IM3** are close in energy, and it is necessary to explore

 © 2007 Wiley-VCH Verlag GmbH & Co. KGaA, Weinheim

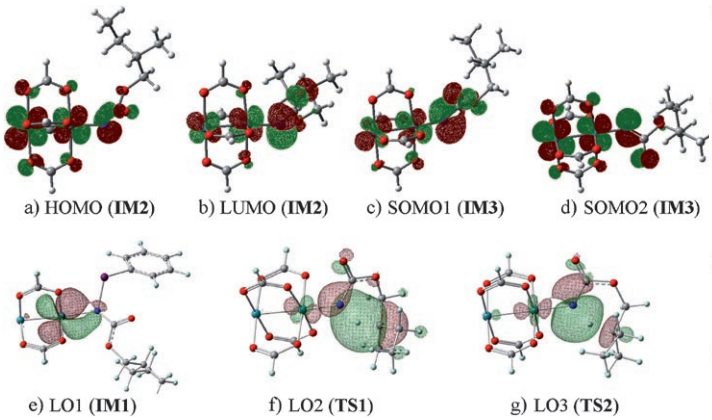

Figure 4. Selected Kohn–Sham orbitals for **IM2** and **IM3**, and localized orbitals for **IM1**, **TS1**, and **TS2**. The contour value is 0.020 e au^{-3}.

the NR-group insertion into the C–H bond through pathways that involve both **IM2** and **IM3**. It was known[32,33] that nitrenes (NR) may be more stable in the singlet than in the triplet state when R is a good π donor; in our case, the π interaction of the metal with the nitrene nitrogen atom stabilizes the singlet state in a similar fashion.

On the basis of the experimental results reported in the literature, we only examined the amidation reactions that form six- or five-membered-ring products by NR-group insertions into primary, secondary, or tertiary C–H bonds. The formation of four- and seven-membered rings was not considered in this work owing to unfavorable ring strains. Six reaction pathways were examined through the location of the transition states and the product complexes associated with **IM2** and **IM3** on the potential-energy surfaces: pathways 1 (singlet) and 2 (triplet) for tertiary, pathways 3 (singlet) and 4 (triplet) for secondary, and pathways 5 (singlet) and 6 (triplet) for primary C–H bond amination. We denote **TS*n*** and **PC*n*** ($n = 1$–6) as the transition state and product complex of the *n*th pathway, respectively, and their geometries are depicted in Figure 5. The free-energy profiles for these reaction pathways are shown in Figure 6.

As depicted in Figure 6, the singlet pathways (pathways 1, 3, 5) are significantly favored over the triplet ones (pathways 2, 4, 6). For instance, the reaction barrier for NR insertion into a tertiary C–H bond for the singlet pathway is 5.6 kcal mol^{-1} lower than that for the corresponding triplet pathway. As **IM2** proceeds to **TS1**, the H(1) atom detaches from the C(3) atom with a C(3)···H(1) distance of 1.252 Å and approaches the N atom with an N···H(1) distance of 1.357 Å. Upon examination of the MO coefficients, the LUMO orbital of **IM2** (Figure 4b) has a large contribution from the N 2p orbital. This makes the N atom of **IM2** strongly electrophilic. The C(3)–H(1) σ bonding electrons are attracted by the vacant N 2p orbital, so that the total charge of the 2-methylbutoxycarbonyl moiety increases significantly from 0.173 for **IM2** to 0.486 for **TS1**, thus indicating that it has hydride-transfer character. The hydride transfer is accompanied by simultaneous formation of the C(3)–N bond as revealed by the local orbital LO2 (Figure 4f) of **TS1**. There is a strong orbital interaction between the C(3) and N atoms, with a trigonal transition-state structure, which indicates that both the hydride transfer and C(3)–N bond formation take place in a concerted manner. This is clearly supported by the structure of **PC1**, which is preceded by **TS1** on the reaction pathway.

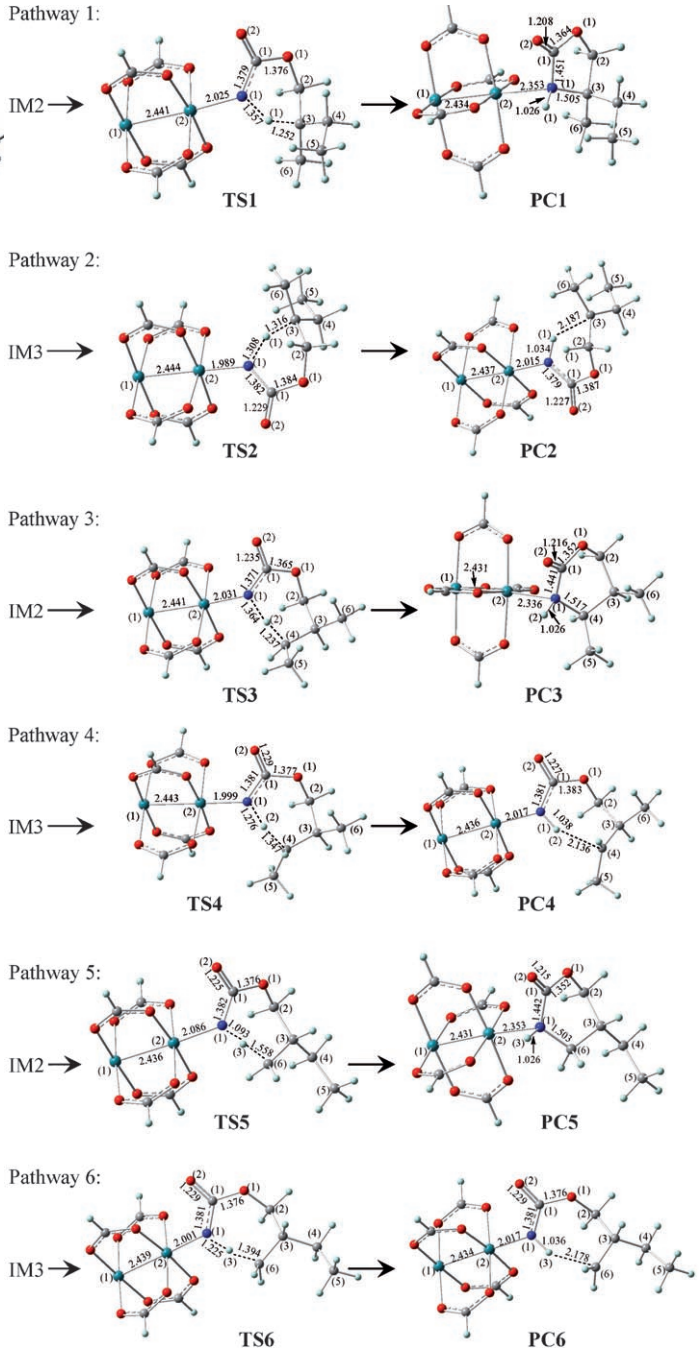

Figure 5. Optimized structures at the BPW91/BS1 level of the transition states and product complexes involved in six proposed pathways for the $Rh_2^{II,II}$-catalyzed intramolecular amination of (*S*)-2-methylbutyl carbamate via intermediates **IM2** and **IM3**. Key bond lengths and distances (Å) are indicated. See text for more details.

 © 2007 Wiley-VCH Verlag GmbH & Co. KGaA, Weinheim

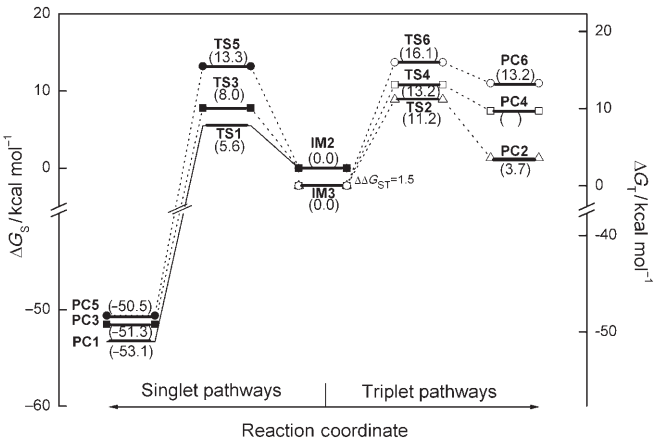

Figure 6. Schematic diagram showing the computed relative free energies (kcal mol^{-1}) at the BPW91/BS1 level for the different reaction pathways in Figure 5. See text for more details. —— = singlet tertiary, ■ = singlet secondary, ● = singlet primary, △ = triplet tertiary, □ = triplet secondary, ○ = triplet primary C–H bond amidation.

The triplet pathway starts from **IM3**, which has two singly occupied MOs with a large N 2p coefficient. The formation of the σ_{N-H} bond would require one electron from the approaching H atom to go to one of the two SOMOs, thus leading to homolytic rather than heterolytic cleavage of the C(3)–H(1) bond. Homolysis of the C(3)–H(1) bond leads to one unpaired electron residing on the C(3) atom and the other residing in the intact SOMO. These suggestions are supported by the results of a spin-density analysis (Table 3).

Table 3. Spin densities for selected atoms in **IM3**, **TS2**, and **PC2** for reaction pathway 2 at the BPW91/BS1 level of theory.

	Rh(1)	Rh(2)	N(1)	O(2)	Rh(1)+Rh(2)+N(1)+O(2)	C(3)	Total
IM3	0.230	0.409	1.098	0.260	1.997	0.004	2.001
TS2	0.308	0.381	0.683	0.191	1.562	0.432	1.994
PC2	0.260	0.335	0.338	0.140	1.074	0.874	1.948

In **IM3**, the spin densities mainly reside on the N (1.098), Rh(1) (0.230), Rh(2) (0.409), and O(2) (0.260) atoms. The total spin density of these four atoms is 1.997, thus indicating a triplet intermediate. The change in spin density mainly occurred at the N and C(3) atoms, and there were relatively small changes in spin density at O(2) and the two Rh atoms. The spin density of the N atom decreased from 1.098 to 0.683, and that of the C(3) atom increased from 0.004 to 0.432 during the **IM3**→**TS2** process. This implies that, as H(1) approaches the N atom, the C(3)–H(1) σ bond undergoes homolytic cleavage. As **TS2** proceeded to **PC2**, the spin density of C(3) increased to 0.874, and the configuration of the C(3) atom changed from a pyramidal to a planar structure to produce **PC2**. The results of the spin-density analysis show that **PC2** is a diradical species. Thus, the N–H(1) bond formation would not be accompanied by C(3)–N bond formation during the **IM3**→**TS2**→**PC2** process. The local orbital LO3 of **TS2** (Figure 4 g) is different from LO2 of **TS1** (Figure 4 f). The H(1) atom interacts covalently with the N atom, whereas the C(3) atom does not interact with the N atom in the transition state. This is supported by the structure found for **PC2**. In the **IM3**→**TS2**→**PC2** process, the cleavage of a C–H bond is accompanied by the formation of a new N–H bond, but in the **IM2**→**TS1**→**PC1** process, the cleavage of a C–H bond is accompanied by the formation of two new σ bonds (C–N and N–H). Because bond formation is exothermic and bond cleavage is endothermic, one might expect that a two-bond formation process is energetically more favorable than the formation of one bond. In other words, the singlet pathway would have a lower activation barrier than the triplet, which is consistent with the results depicted in Figure 6. Structurally, the C(3)···H(1) distance of 1.316 Å in **TS2** is longer than that of 1.252 Å in **TS1**, and the N···H(1) distance of 1.308 Å in **TS2** is shorter than that of 1.361 Å in **TS1**. The geometry change from **IM3** to **TS2** is larger than that from **IM2** to **TS1**, which also suggests that the triplet pathway has a higher activation energy barrier.

PC1 is formed from the $Rh_2^{II,II}$ catalyst and the oxazolidinone product with the configuration of the C(3) atom retained during the nitrene-insertion reaction. Its subsequent decomposition to give the enantiomerically pure product (*S*)-4-ethyl-4-methyloxazolidin-2-one (**3** in Figure 1) and the starting $Rh_2^{II,II}$ catalyst could be facile. The free-energy change for this decomposition process was found to be −2.0 kcal mol^{-1} at the BPW91/BS1 level of theory. **PC2** has a different structural character to **PC1**, but is rather similar to **TS2** in structure. The C(3)–N bond does not form in **PC2**, although the N–H(1) bond is formed with a bond length of 1.034 Å. The C(3) atom has sp^2-hybridization character, and the vicinal moiety of the C(3) atom exhibits a roughly planar structure. The rate of recombination of diradical species **PC2**, that is, C(3)–N bond formation, depends on the rate of its state crossing from triplet to singlet when C(3) approaches the N atom. However, due to the rotation of the planar $CH_2C(CH_3)CH_2CH_3$ moiety, the C(3) atom may not retain its original configuration, and this could lead to decreased stereoselectivity in the formation of the oxazolidinone product from **PC2**. The singlet and triplet pathways gave similar results for the amination of secondary or primary C–H bonds. Thus, in the Rh-mediated concerted singlet nitrene insertion, the amidation product is generated with retention of chirality, whereas in the triplet nitrene stepwise pathway, the diradical intermediate **PC2** is first formed, followed by subsequent recombination (Scheme 2). The concerted mechanism with the singlet pathway and the stepwise mechanism with the triplet pathway for nitrene insertion are similar to the case of the P450-enzyme-catalyzed hydroxylation reactions reported previously.[43]

The relative reaction rates for the singlet pathways over the triplet may be estimated according to transition-state theory by Equation (1):

$$k_{singlet}/k_{triplet} \approx \exp[(\Delta G^{\neq}{}_{triplet} - \Delta G^{\neq}{}_{singlet} + \Delta G_{st})/RT] \qquad (1)$$

As listed in Table 4, the relative reaction rates ($k_{singlet}/k_{triplet}$) for the amidation of tertiary, secondary, and primary

 © 2007 Wiley-VCH Verlag GmbH & Co. KGaA, Weinheim

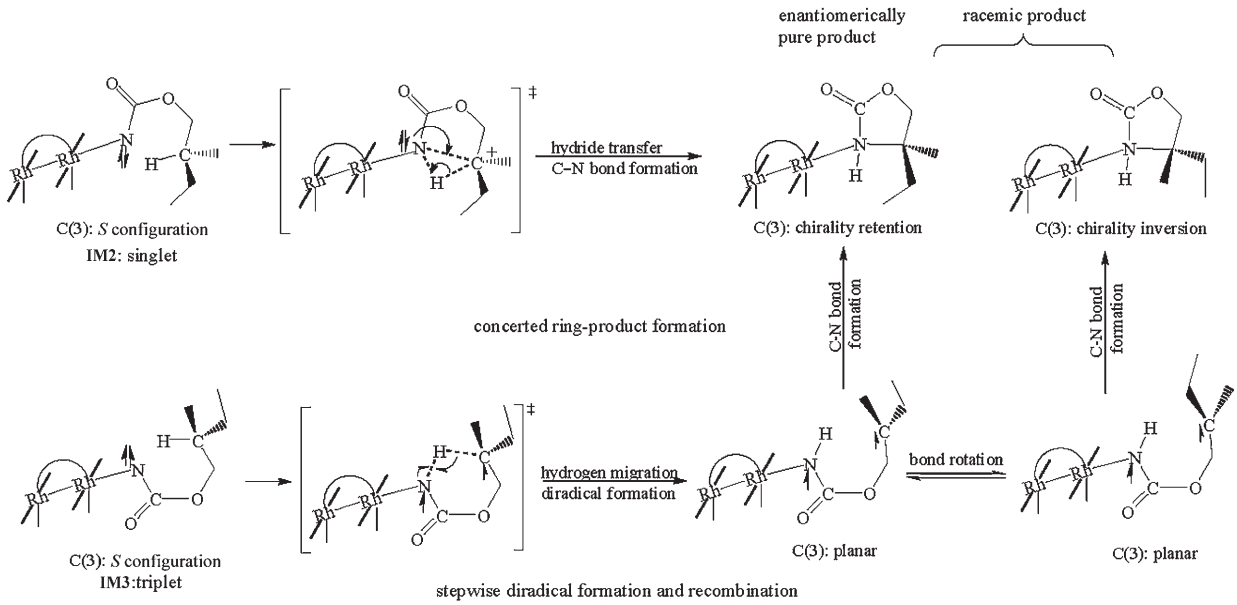

Scheme 2. Proposed concerted singlet insertion and stepwise triplet recombination mechanisms for the $Rh_2^{II,II}$-mediated amidation reaction.

C–H bonds were 7.3×10^2, 3.8×10^2, and 8.1, respectively. Inclusion of bulk solvation (CH_2Cl_2) effects on the reactions at different computational levels gave rather similar $k_{singlet}/k_{triplet}$ data. All the results obtained with these different methods indicate that the singlet concerted pathway is the predominant pathway, which is responsible for the formation of the enantiomerically pure oxazolidinone product.[13]

N-Atom Insertion into Different C–H Bonds: Regioselectivity

In the literature, it has been shown that in $Rh_2^{II,II}$-catalyzed C–N bond-formation reactions, the nitrene will preferentially insert into tertiary and benzylic C–H bonds,[1,3,14] and that the formation of five/six-membered rings is favored.[1,11,13,14,25] As described in the previous section, the rate constants for the singlet pathways are larger than the corresponding ones for the triplet pathways. Thus, we focused our further analysis on the singlet pathways, that is, pathways 1, 3, and 5. **TS1** is a six-membered-ring transition state, whereas **TS3** and **TS5** are seven-membered-ring transition states. The geometry change from **IM2** to **TS3** is smaller than that from **IM2** to **TS5**, which implies that there is a lower energy barrier for the former pathway. From Figure 6, singlet tertiary C–H bond insertion (pathway 1) is the most favorable pathway with an activation barrier of 5.6 kcal mol^{-1}, which is 2.4 kcal mol^{-1} lower than that for singlet secondary C–H bond insertion, and 7.7 kcal mol^{-1} lower than that for singlet primary C–H bond insertion. The order of reactivity for the singlet concerted pathways of C–H bond amidations is tertiary > secondary > primary C–H bonds. The singlet concerted pathways have some hydride-transfer character, which results in a significant increase in the charge on the 2-methylbutoxycarbonyl moiety. Its charge increased by 0.313, 0.337, and 0.537 from **IM2** to **TS1**, **TS3**, and **TS5**, respectively. This reveals that the charge increase is in correlation with the energy barrier for the singlet reaction pathways. The hydride-transfer character of the singlet concerted pathways also implies that the nitrene favors insertion into C–H bonds that have vicinal groups to stabilize the positive charge of the carbon atom. Therefore, the tertiary C–H bond is the most favorable site. This is in good agreement with experimental results reported by various workers.[1,3,14,25] The level of regioselectivity can also be esti-

Table 4. Energy and free-energy barriers and estimated relative reaction rates of the different reaction pathways.

Reactions[a]	BPW91/BS1				BPW91/BS1/DPCM				BPW91/BS3/DPCM//BPW91/BS1			
	$\Delta E^{\neq}$ [kcal mol^{-1}]	$\Delta G^{\neq}$ [kcal mol^{-1}]	$k_{si}/k_{t(i+1)}$[b]	k_1/k_j[c]	$\Delta E^{\neq}$ [kcal mol^{-1}]	$\Delta G^{\neq}$ [kcal mol^{-1}]	$k_{si}/k_{t(i+1)}$[b]	k_1/k_j[c]	$\Delta E^{\neq}$ [kcal mol^{-1}]	$\Delta G^{\neq}$ [kcal mol^{-1}]	$k_{si}/k_{t(i+1)}$[b]	k_1/k_j[c]
Pathway 1	3.8	5.6	7.3×10^2	1	4.5	3.2	1.9×10^3	1	4.0	3.5	1.0×10^3	1
Pathway 2	9.8	11.2		7.3×10^2	11.7	9.3		1.9×10^3	10.4	9.3		1.0×10^3
Pathway 3	5.6	8.0	3.8×10^2	47	6.7	6.2	5.3×10^2	1.2×10^2	6.9	6.5	3.3×10^2	1.2×10^2
Pathway 4	11.4	13.2		1.8×10^4	13.7	11.5		6.5×10^4	12.9	11.6		8.1×10^3
Pathway 5	11.9	13.3	8.1	2.4×10^5	10.5	8.7	90	6.9×10^3	9.7	9.0	47	6.9×10^3
Pathway 6	14.3	16.1		1.9×10^6	15.8	12.9		6.2×10^5	14.4	12.9		3.3×10^5

[a] The reaction pathways are described in Figure 4. [b] k_{si} represents the reaction rate constant for the singlet pathway in pathway i, and $k_{t(i+1)}$ represents the reaction rate constant for the triplet pathway in pathway $(i+1)$, in which $i=1$, 3, 5. [c] k_j represents the relative reaction rate constant for pathway j with respect to pathway 1, in which $j=1$–6.

 © 2007 Wiley-VCH Verlag GmbH & Co. KGaA, Weinheim

mated by the relative reaction rates of N atom insertion into different C–H bonds [Eq. (2)]:

$$k_{\text{singlet},2}/k_{\text{singlet},1} = \exp[(\Delta G^{\neq}{}_{\text{singlet},1} - \Delta G^{\neq}{}_{\text{singlet},2})/\text{RT}] \quad (2)$$

As shown in Table 4, the singlet concerted pathway for tertiary C–H bond insertion to afford the chirality-retention product is the most favorable of these six pathways. The relative reaction rate for pathway 1 is so much larger than those for pathways 2, 4, 5, and 6 that these latter four pathways probably do not play any significant role. The relative reaction rate of pathway 1 to pathway 3 (k_1/k_3) is about 47 at the BPW91/BS1 level of theory, and is 1.2×10^2 when solvation effects are considered. This enables the amidation reaction to occur at the tertiary C atom to give the product in high yield. This is consistent with experimental observations.[13]

Conclusions

In summary, we propose a mechanistic framework for the $Rh_2^{II,II}$-catalyzed intramolecular amination of carbamates. The $Rh_2^{II,II}$–nitrene complex(es) (**IM2**/**IM3**) rather than the $Rh_2^{II,II}$–pheyliodinane complex (**IM1**) is responsible for delivery of the NR group. The concerted singlet reaction pathways via **IM2** lead to retention of the configuration of the carbon atom in the oxazolidinone product, and the stepwise triplet diradical recombination pathways via **IM3** may lead to the formation of racemic products. Although the singlet (**IM2**) and triplet (**IM3**) intermediates have similar thermodynamic stability, the NR-group-insertion step preferentially proceeds via **IM2** owing to a lower activation barrier than via **IM3**. The order of reactivity for the singlet concerted pathways is tertiary > secondary > primary C–H bonds. The overall regioselectivity computed in this work is consistent with the experimental results reported by Espino and Du Bois.[13] It would be interesting to study other relevant reactions, such as the Rh-catalyzed amination of sulfamates,[12,14] or other transition-metal-catalyzed amination or aziridination reactions[1,3,25,44,45] to help explain/predict the selectivity of these reactions.

Computational Details

DFT with the 1988 Becke exchange[34] and the Perdew and Wang correlation[46] functionals was used to examine the potential-energy surfaces of the $Rh_2^{II,II}$-catalyzed NR-group insertion into C–H bonds. Geometry optimization and frequency analysis were done with the Gaussian 98 software suit (Version A7).[47] The restricted DFT method was used for calculation of singlet-state structures, and the unrestricted DFT method was used for triplet-state structures. Three levels of basis sets, denoted BS1–BS3, were used in this work. For all C, H, and O atoms, the 6-31G* basis set was used in BS1, the 6-31G basis set was used in BS2, and the 6-311++G(d,p) basis set was used in BS3. For the N atom, the 6-31G* basis set was used in BS1 and BS2, and the 6-311++G(d,p) basis set was used in BS3. For the Rh atom, the LANL2DZ[48] basis set was used in BS1 and BS2, and the SDD[49] basis set was used in BS3. For the I atom, the LANL2DZ basis set in conjunction with diffuse and polarization functions (LANL2DZdp)[50] was used in all basis sets. As CH_2Cl_2 is a commonly used solvent for $Rh_2^{II,II}$-catalyzed NR insertion into C–H bonds, the effect of bulk solvation was examined with the polarized continuum solvation model (D-PCM)[51–53] (implemented in the latest version of Gaussian 03) utilized for CH_2Cl_2 ($\varepsilon = 8.30$ at 313.15 K). Bondi atomic radii[54] were used in the D-PCM calculations, in which the H atoms were explicitly considered to build up the solvation cavity. Intrinsic reaction coordinate (IRC) calculations were done to confirm that the transition states proposed connected the appropriate reactants and products.[55] The Cartesian coordinates, total energies, and vibrational zero-point energies for the computed structures are given in the Supporting Information.

Acknowledgements

We are grateful for financial support from the Research Grants Council (HKU 7011/04P), the University Grant from the Sun Yat-Sen University, and the Areas of Excellence Scheme established under the University Grants Committee of the Hong Kong Special Administrative Region, China (AoE/P-10/01).

[1] H. M. Davies, M. S. Long, *Angew. Chem.* **2005**, *117*, 3584; *Angew. Chem. Int. Ed.* **2005**, *44*, 3518.
[2] P. Müller in *Advances in Catalytic Processes*, *Vol. 2*, *Asymmetric Catalysis* (Ed.: M. P. Doyle), JAI Press, Greenwich, **1997**.
[3] P. Müller, C. Fruit, *Chem. Rev.* **2003**, *103*, 2905.
[4] R. Breslow, S. H. Gellman, *J. Chem. Soc. Chem. Commun.* **1982**, 1400.
[5] R. Breslow, S. H. Gellman, *J. Am. Chem. Soc.* **1983**, *105*, 6728.
[6] J. P. Mahy, G. Bedi, P. Battioni, D. Mansuy, *New J. Chem.* **1989**, *13*, 651.
[7] P. Dauban, R. H. Dodd, *Org. Lett.* **2000**, *2*, 2327.
[8] P. Dauban, L. Saniere, A. Tarrade, R. H. Dodd, *J. Am. Chem. Soc.* **2001**, *123*, 7707.
[9] P. Müller, C. Bolea, *Helv. Chim. Acta* **2002**, *85*, 483.
[10] K. W. Fiori, J. J. Fleming, J. Du Bois, *Angew. Chem.* **2004**, *116*, 4449; *Angew. Chem. Int. Ed.* **2004**, *43*, 4349.
[11] P. M. Wehn, J. H. Lee, J. Du Bois, *Org. Lett.* **2003**, *5*, 4823.
[12] C. G. Espino, K. W. Fiori, M. Kim, J. Du Bois, *J. Am. Chem. Soc.* **2004**, *126*, 15378.
[13] C. G. Espino, J. Du Bois, *Angew. Chem.* **2001**, *113*, 618; *Angew. Chem. Int. Ed.* **2001**, *40*, 598.
[14] C. G. Espino, P. M. Wehn, J. Chow, J. Du Bois, *J. Am. Chem. Soc.* **2001**, *123*, 6935.
[15] J. J. Fleming, K. W. Fiori, J. Du Bois, *J. Am. Chem. Soc.* **2003**, *125*, 2028.
[16] I. Nageli, C. Baud, G. Bernardinelli, Y. Jacquier, M. Moran, P. Müller, *Helv. Chim. Acta* **1997**, *80*, 1087.
[17] P. M. Wehn, J. Du Bois, *J. Am. Chem. Soc.* **2002**, *124*, 12950.
[18] J. L. Liang, J. S. Huang, X. Q. Yu, N. Y. Zhu, C. M. Che, *Chem. Eur. J.* **2002**, *8*, 1563.
[19] Y. Kohmura, T. Katsuki, *Tetrahedron Lett.* **2001**, *42*, 3339.
[20] J. P. Mahy, G. Bedi, P. Battioni, D. Mansuy, *Tetrahedron Lett.* **1988**, *29*, 1927.
[21] X. Q. Yu, J. S. Huang, X. G. Zhou, C. M. Che, *Org. Lett.* **2000**, *2*, 2233.
[22] S. M. Au, J. S. Huang, C. M. Che, W. Y. Yu, *J. Org. Chem.* **2000**, *65*, 7858.
[23] S. M. Au, S. B. Zhang, W. H. Fung, W. Y. Yu, C. M. Che, K. K. Cheung, *Chem. Commun.* **1998**, 2677.
[24] J. L. Liang, X. Q. Yu, C. M. Che, *Abstr. Pap. Am. Chem. Soc.* **2002**, *224*, U712.
[25] J. L. Liang, S. X. Yuan, J. S. Huang, W. Y. Yu, C. M. Che, *Angew. Chem.* **2002**, *114*, 3615; *Angew. Chem. Int. Ed.* **2002**, *41*, 3465.
[26] X. G. Zhou, X. Q. Yu, J. S. Huang, C. M. Che, *Chem. Commun.* **1999**, 2377.

 © 2007 Wiley-VCH Verlag GmbH & Co. KGaA, Weinheim

[27] C. Ohta, T. Katsuki, *Tetrahedron Lett.* **2001**, *42*, 3885.
[28] S. M. Au, J. S. Huang, W. Y. Yu, W. H. Fung, C. M. Che, *J. Am. Chem. Soc.* **1999**, *121*, 9120.
[29] E. Nakamura, N. Yoshikai, M. Yamanaka, *J. Am. Chem. Soc.* **2002**, *124*, 7181.
[30] N. P. Gritsan, M. S. Platz, W. T. Borden in *Computational Methods in Photochemistry*, *Vol. 13* (Ed.: A. G. Kutateladze), Taylor and Francis, **2005**, chap. 5, p. 235.
[31] A. D. Becke, *J. Chem. Phys.* **1993**, *98*, 5648.
[32] E. A. Pritchina, N. P. Gritsan, T. Bally, T. Autrey, Y. Liu, Y. Wang, J. P. Toscano, *Phys. Chem. Chem. Phys.* **2003**, *5*, 1010.
[33] E. A. Pritchina, N. P. Gritsan, T. Bally, *Russian Chem. Bull.* **2005**, *54*, 525.
[34] A. D. Becke, *Phys. Rev. A* **1988**, *38*, 3098.
[35] O. Castell, V. M. Carefa, C. Bo, R. Caballol, *J. Comput. Chem.* **1996**, *17*, 42.
[36] M. J. Travers, D. C. Cowles, E. P. Clifford, G. P. Eillison, *J. Am. Chem. Soc.* **1993**, *115*, 10857.
[37] The BHandH method used the functional $0.5\times E_X^{HF}+0.5\times E_X^{LSDA}+E_C^{LYP}$.
[38] F. A. Cotton, B. G. Deboer, M. D. Laprade, J. R. Pipal, D. A. Ucko, *Acta Crystallogr. Sect. B* **1971**, *27*, 1664.
[39] a) R. C. Haddon, G. R. J. Williams, *Chem. Phys. Lett.* **1976**, *42*, 453; b) S. F. Boys in *Quantum Theory of Atoms, Molecules, and the Solid State* (Ed.: P. O. Lowdin), Academic Press, New York, **1968**.
[40] M. C. Pirrung, H. Liu, A. T. Morehead, *J. Am. Chem. Soc.* **2002**, *124*, 1014.
[41] M. C. Pirrung, A. T. Morehead, *J. Am. Chem. Soc.* **1994**, *116*, 8991.
[42] W. Kohn, L. J. Sham, *Phys. Rev.* **1965**, *140*, A1133.
[43] B. Meunier, J. Bernadou, *Top. Catal.* **2002**, *21*, 47.
[44] K. Guthikonda, J. D. Bois, *J. Am. Chem. Soc.* **2002**, *124*, 13672.
[45] J. L. Liang, S. X. Yuan, J. S. Huang, C. M. Che, *J. Org. Chem.* **2004**, *69*, 3610.
[46] J. P. Perdew, K. Burke, Y. Wang, *Phys. Rev. B* **1996**, *54*, 16533.
[47] M. J. Frisch, H. B. Schlegel, G. E. Scuseria, M. A. Robb, J. R. Cheeseman, V. G. Zakrzewski, J. A. Montgomery, Jr., R. E. Stratmann, J. C. Burant, S. Dapprich, J. M. Millam, A. D. Daniels, K. N. Kudin, M. C. Strain, O. Farkas, J. Tomasi, V. Barone, M. Cossi, R. Cammi, B. Mennucci, C. Pomelli, C. Adamo, S. Clifford, J. Ochterski, G. A. Petersson, P. Y. Ayala, Q. Cui, K. Morokuma, N. Rega, P. Salvador, J. J. Dannenberg, D. K. Malick, A. D. Rabuck, K. Raghavachari, J. B. Foresman, J. Cioslowski, J. V. Ortiz, A. G. Baboul, B. B. Stefanov, G. Liu, A. Liashenko, P. Piskorz, I. Komaromi, R. Gomperts, R. L. Martin, D. J. Fox, T. Keith, M. A. Al-Laham, C. Y. Peng, A. Nanayakkara, M. Challacombe, P. M. W. Gill, B. Johnson, W. Chen, M. W. Wong, J. L. Andres, C. Gonzalez, M. Head-Gordon, E. S. Replogle, J. A. Pople, Gaussian 98 (Revision A.11.4), Gaussian, Inc., Pittsburgh, PA (USA), **2002**.
[48] P. J. Hay, W. R. Wadt, *J. Chem. Phys.* **1985**, *82*, 299.
[49] M. Dolg, H. Stoll, H. Preuss, R. M. Pitzer, *J. Phys. Chem.* **1993**, *97*, 5852.
[50] C. E. Check, T. O. Faust, J. M. Bailey, B. J. Wright, T. M. Gilbert, L. S. Sunderlin, *J. Phys. Chem. A* **2001**, *105*, 8111.
[51] S. Miertus, E. Scrocco, J. Tomasi, *Chem. Phys.* **1981**, *55*, 117.
[52] S. Miertus, J. Tomasi, *Chem. Phys.* **1982**, *65*, 239.
[53] M. Cossi, V. Barone, R. Cammi, J. Tomasi, *Chem. Phys. Lett.* **1996**, *255*, 327.
[54] A. Bondi, *J. Phys. Chem.* **1964**, *68*, 441.
[55] a) C. Gonzalez, H. B. Schlegel, *J. Chem. Phys.* **1989**, *90*, 2154; b) C. Gonzalez, H. B. Schlegel, *J. Phys. Chem.* **1990**, *94*, 5523.

Received: February 23, 2007
Published online: August 21, 2007

 © 2007 Wiley-VCH Verlag GmbH & Co. KGaA, Weinheim